Cytometry Part A 69A:920–929 (2006)

A New Configuration of the Zeiss LSM 510 for Simultaneous Optical Separation of Green and Red Fluorescent Protein Pairs

Kurt I. Anderson,[1]* Jeremy Sanderson,[2] Silke Gerwig,[3] and Jan Peychl[3]

[1]Beatson Institute for Cancer Research, Glasgow, United Kingdom
[2]Light Microscopy, Department of Biomedical Science, Western Bank, Sheffield, United Kingdom
[3]Light Microscopy Facility, Max Planck Institute of Molecular Cell Biology and Genetics, Dresden, Germany

Received 15 August 2005; Revision Received 11 May 2006; Accepted 22 May 2006

The power and simplicity of genetically encoded fluorophores (fluorescent proteins, FPs) have drawn many molecular biologists to light microscopy. First generation FPs suffered from overlapping excitation and emission spectra, which limited their use together in pairs (Patterson et al., J Cell Sci 2001;114 (Part 5):837–838). Image acquisition and processing techniques, collectively known as linear unmixing, have been developed to separate overlapping fluorescence signals encountered in the imaging of FP pairs and also in FRET. These specialized techniques are not without their potential drawbacks, including limitations on sensitivity and time-resolution for live cell imaging, and the risk of artifact in the hands of nonspecialists. With the advent of a new generation of red-shifted FPs (Shaner et al., Nat Biotechnol 2004;22:1567–1572; Verkhusha and Lukyanov, Nat Biotechnol 2004;22:289–296) careful selection of excitation sources and emission filters obviate the need for linear unmixing when simple two channel imaging of FPs is required. Here we introduce a new configuration of the Zeiss LSM 510 laser scanning confocal microscope, optimized for live cell imaging of green fluorescent protein (GFP) together with spectral variants such as mRFP1 and mCherry using standard photo-multipliers. A 2 mW, 594 nm HeNe laser was chosen as the excitation source for the red FP. This wavelength efficiently excites the aforementioned red variants without limiting the detection range of GFP emission during simultaneous two-channel imaging. Compared to excitation of GFP and mCherry at 488 and 543 nm, excitation at 488 and 594 nm approximately doubles the sensitivity of GFP detection and eliminates bleed-through of GFP into the mCherry channel. However, sensitivity of mCherry detection is decreased by 30%, suggesting the need for red FPs having longer emission peaks. Practical advantages to the simultaneous optical separation of FPs with nonoverlapping emission spectra include simplicity, robustness, reduced risk of artifact, and increased sensitivity during live cell imaging. © 2006 International Society for Analytical Cytology

Key terms: laser scanning confocal microscopy; green fluorescent protein, GFP; red fluorescent protein, mRFP1; mCherry; HeNe laser 594 nm; linear unmixing

In the 1960s, development of epi-fluorescence microscopy was driven by the application of antibody labeling to localize proteins in fixed specimens. Techniques for live cell fluorescence microscopy followed in the 1970s and 80s; however, their utility was limited by the range of available fluorophores and substantially constrained by the available methods for introducing active, labeled biomolecules into living cells (1,2). The cloning of green fluorescent protein (GFP) (3,4) subsequently launched a revolution in cell and developmental biology based on the unparallel specificity and sensitivity for labeling structures within cells and tissues. Fluorescent protein (FP) constructs (5–7) have become widely used genetic tools to address fundamental questions of the recruitment, co-localization, and interactions of specific proteins within subcellular compartments. Truly, novel insights have resulted from experiments based on live cell imaging, which would be difficult if not impossible to achieve through the observation of fixed specimens. The use of fluorescence recovery after photo-bleaching to demonstrate actin filament treadmilling in fibroblast lamellipodia is one such example (8). Other examples include the observation of

The four authors of this paper have no commercial or financial interests with any company or manufacturer cited herein, neither do they have any affiliation with any company or manufacturer, either at the time of the design and commissioning of this new configuration, or subsequently at the submission of this paper for publication.

*Correspondence to: Kurt I. Anderson, Beatson Institute for Cancer Research, Garscube Estate, Switchback Road, Glasgow, G61 1BD, UK.
E-mail: k.anderson@beatson.gla.ac.uk

Published online in Wiley InterScience (www.interscience.wiley.com).
DOI: 10.1002/cyto.a.20323

transient, repeated interactions between microtubules and focal adhesions (9), the sequential recruitment of clathrin, WASP and actin to endocytic sites on the plasma membrane (10), and the growth of actin meshworks across the dictyostelium cell surface (11). Rapid image acquisition is often critically important to properly resolve dynamic events. Photobleaching, however, generally limits the total number of images which can be derived from a living sample. Thus, live cell imaging of weak fluorescent signals, at a given time resolution, with a given signal to noise ratio, for the duration of an experiment, often requires optimization of every possible image acquisition parameter.

The initial rapid expansion of the available palette (or "rainbow") of high-contrast intrinsically FP markers transformed cell and developmental biology, with multi-label fluorescent imaging of living specimens assuming a place of prime importance (12,13). The first generation of FPs developed after GFP (BFP, CFP, YFP, dsRed, and variants, reviewed by Patterson, 2001) suffered from a variety of shortcomings, which limited their usefulness in multi-label applications, especially when maximum sensitivity to low signals was required (14). These proteins and their properties have been extensively reviewed (15). Shortcomings include poor quantum yield, low photo-stability, the proclivity to aggregate, and overlapping excitation and emission spectra (16,17). Although the first three shortcomings might limit the ability to conduct an experiment, overlapping emission spectra are instead more likely to lead to a wrong answer; a false positive of co-localization resulting from cross-talk between two signals. This danger is increased among novice microscopists, who require simple and robust procedures to insure successful, reproducible results. The simplest and most robust approach to limiting fluorescence crosstalk is to use fluorophores with nonoverlapping emission spectra. This approach also maximizes sensitivity by detecting each fluorophore over the widest possible emission range. This has the indirect effect of extending sample longevity through reduced photo-damage.

Our goal was to specify an optimal laser scanning configuration for simple, robust, two channel live cell imaging of a green FP and a longer wavelength fluorophore in metazoan cells, a common important application of many imaging facilities. Maximum sensitivity of detection was a priority to allow imaging of live specimens at good signal to noise levels, over long time periods, with high time resolution. The system was designed for demanding applications in live cell imaging, which are often undertaken by nonimaging specialists. There are necessarily many applications for which this configuration has not been optimized, foremost among them FRET in its many forms. Simplicity, robustness, and sensitivity are rooted in the selection of fluorophores with nonoverlapping emission spectrum.

MATERIALS AND METHODS

Modification of Zeiss LSM 510

The Zeiss LSM 510 confocal system, hardware version 3.2, was modified in cooperation with the Microscopy Division's product management team at Carl Zeiss Jena (Germany). We exchanged the green 543 nm HeNe laser with the orange 594 nm HeNe laser, and specified new primary and secondary beamsplitters as well as emission filters for the three standard photo-multiplier (PMT) detection channels. An important challenge was to make the best use of the limited number of positions available within the filter wheels. Our goal was to cover the most frequently used and potentially requested imaging applications for the users of our imaging facility. The final configuration is presented in Figure 1.

Selection of Primary and Secondary Beamsplitters

Hard-coated filters were chosen for high overall transmission. Conventional "soft-coated" filters, especially primary beam-splitters, typically suffer from lower overall transmission efficiency, as more lines of reflection are added. A rule of thumb is a loss of 5% transmission efficiency for each additional laser line to be used with the mirror. Thus, a single line primary beamsplitter such as the HFT 488 might have around 95% transmission of GFP fluorescence, whereas the HFT 488/543/633 triple beamsplitter would have had lower fluorescence transmission, perhaps around 80%. However, thanks to improvements in mirror design and coating technology, double and triple band-pass dichroics can now be designed, which have transmission efficiency as high as single line mirrors. Therefore, our configuration has only an HFT 405/488/594 but no HFT 488/594. Reflection at 405 has no impact on experiments using only 488 and 594 nm excitation, and the transmission efficiency of the mirror is equal to the 488/594 beamsplitter for the detection of green and red fluorescence.

FP Constructs

GFP emission data was collected using the AcGFP1-actin vector (Clonetech) expressed in B16 cells (kindly prepared by Ireen König). For the GFP detection range, MDCK cells expressing VSV-G-GFP (pEGFP-C3, Clontech) (18) were used (kindly donated by Sebastian Schuck). mCherry emission data was collected using mCherry expressed in FBR fibroblasts either cytoplasmically (for emission spectrum, kindly donated by Lynn McGarry) or as a LASP chimera (for detection range, kindly donated by Heather Spence).

Collection of Emission Spectra

GFP and mCherry emission spectra. Images were acquired using an Olympus FV1000 confocal scanhead mounted on an IX-81 inverted microscope using a 60× 1.35 NA UPLANSAPO objective. The 405/488 primary dichroic was selected and each probe excited in separate samples at 405 nm. Use of the 405/488 primary splitter allowed for emission to be collected over the range of 500–700 nm with no signal loss due to reflection of the splitter for other laser lines.

GFP detection range. Images were acquired on two different Zeiss LSM 510 inverted confocal microscope sys-

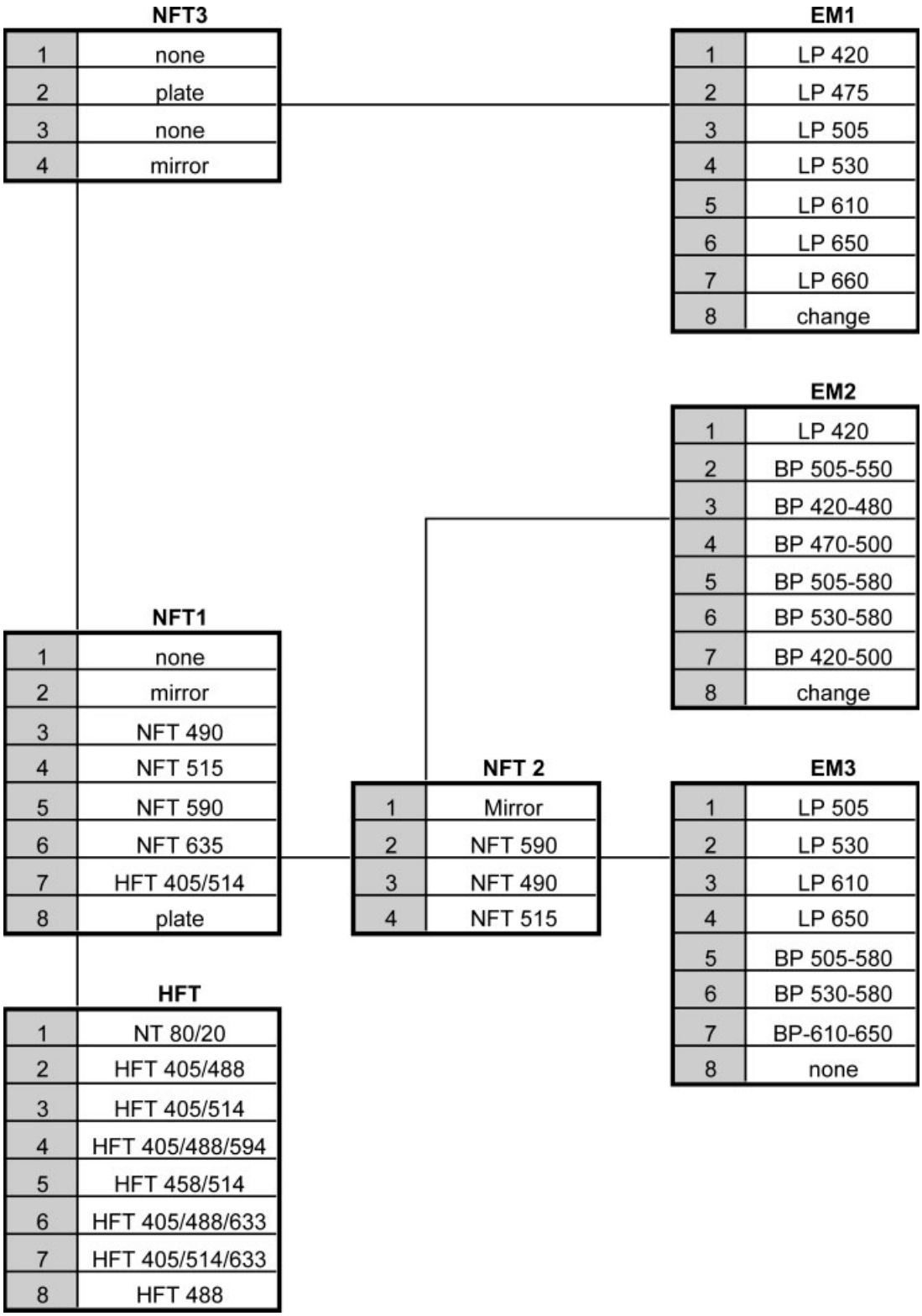

FIG. 1. Filter configuration. This configuration of the Zeiss LSM 510 was specified for simultaneous imaging of GFP and mCherry. HFT stands for Hauptfarbteiler, the primary beam splitter position that reflects laser light onto the sample for fluorescence excitation and allows the associated emission to pass back toward the detector. NFT stands for Nebenfarbteiler, or secondary beam splitter, which directs fluorescence emission from the sample toward the three PMT detectors. Emission filters in the three EM positions block unwanted light, such as reflected laser light and crosstalk from other fluorophores.

tems using the same Plan-Apochromat 63× 1.4 NA objective, excited at 488 nm. A system having 488 and 543 nm excitation lines was used to detect GFP emission at 505–550 and 505–530 nm. A system having excitation lines at 488 and 594 nm was used to detect GFP emission at 505–580 nm. GFP was detected using a LP 505 emission filter on both systems, and this image was used to normalize intensities presented in Figure 3.

mCherry detection range. Images were acquired using a Leica TCS SP2 inverted confocal system with AOBS using an HC PLANAPO 63× 1.4 NA objective. mCherry was excited using 543 nm and detected in typical red detection channels of 550–700, 575–700, 605–700, and 610–700 nm.

GFP crosstalk. Images were acquired using a Leica TCS SP2 inverted confocal system with AOBS using an HC PLANAPO 63× 1.4 NA objective. GFP was excited at 488 nm and detected at 500–530 nm. GFP signal was also detected in typical red channels of 550–700, 575–700, 605–700, and 610–700 nm. The PMT gain setting of both green and red channels was held constant at 650, and laser power was varied to produce a strong signal in the green channel (500–530 nm).

In all cases where the same sample was imaged repeatedly, photobleaching was checked to be less than 5% over the course of the experiment.

Laser Power Measurement

To quantify the power of the three lasers fitted to the system (Argon-ion, He-Ne 594 nm and He-Ne 633 nm), the laser power was measured directly in two different locations. The first measurement was performed at the laser head, before any attenuation through the mirrors, AOTF, couplings, and fibers of the optical pathway. Laser power was also measured at the object plane through a 10× NA 0.3 Plan Neofluar objective (Zeiss, Germany), 80/20 dichroic mirror using the HWAdminEx macro (Zeiss) according to the company protocol. At the time of measurement, all lasers were roughly 1 year old—having approximately 2000 h of use. Before measurement, all the lasers were switched on and allowed to equilibrate for at least 2 h. The temperature within the laser room was recorded at the time of measurement and ranged from 23.4 to 24.6°C, which was within acceptable limits. For the duration of each measurement, the argon-ion laser was run at 8.1 A from within the AIM software. All measurements were performed eight times (once per week) using a Lasermate Q (Coherent, USA) power meter, which had been set to the appropriate wavelength, using the VIS detector head (which covers 405 nm, see also Ref. 19).

RESULTS

Fluorophore Selection

When choosing a fluorochrome for use with GFP, it is helpful to begin by considering the emission spectrum of GFP, which peaks around 510 nm but trails off toward 600 nm (Fig. 2). In the confocal microscope the intensity

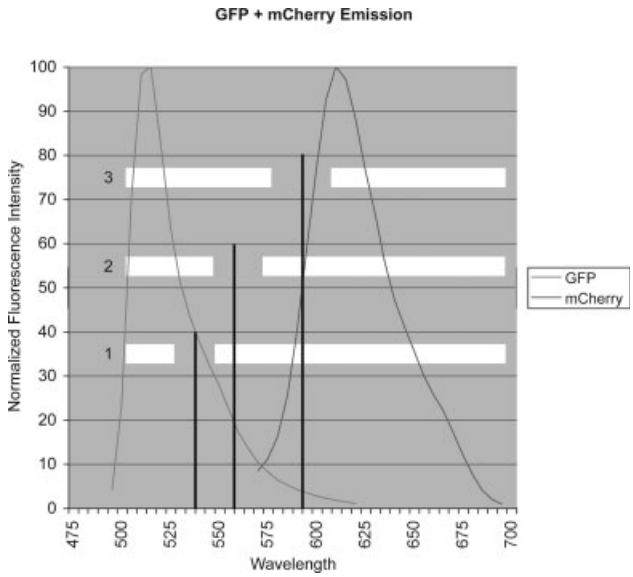

FIG. 2. GFP and mCherry emission spectra. GFP and mCherry were excited in separate samples using 405 nm laser light and a 405/488 primary dichroic. Excitation at 405 was chosen to collect the widest possible emission range, using a primary beamsplitter with a single, broad transmission range from 488 nm past 700 nm. Laser lines for red excitation are indicated by vertical lines at 543, 561, and 594 nm. White bars represent three detection channel pairs for green and red imaging, which have been laid over the emission spectra: (1) (488/543) excitation of green and red at 488 and 543 nm, detection of green at 505–530 nm, detection of red at 550–700 nm; (2) (488/561) excitation of green and red at 488 and 561 nm, detection of green at 505–550 nm, detection of red at 575–700 nm; (3) (488/594) excitation of green and red 488 and 594 nm, detection of green at 505–580, detection of red at 610–700 nm.

of GFP emission is less than 10% of the peak value below 495 nm and above 570 nm, meaning that the spectral range of conventionally detectable GFP emission is around 75 nm. A red FP for use with GFP should ideally have an emission peak well above 580 nm to insure that the early part of the red peak does not overlap with the trailing part of the GFP emission. This circumvents problems of bleed-through of the second excitation wavelength into the GFP channel (see later) and reduced sensitivity due to the use of double bandpass primary beamsplitters when sequential scanning is used (see Discussion). A number of red FP variants have been derived from the anthozoan protein dsRed (20), which appear suitable for use with GFP in dual color imaging applications, including a monomeric variant (mRFP1) prepared by Campbell (21), a subsequent variant (mRFPmars) produced by Fischer (22), and several variants introduced by Shaner (23). Despite a marginal theoretical loss in resolution, which may be unnoticeable in practice, there are several advantages to using longer wavelength fluorophores in combination with GFP: less light scattering through cells and tissues; less photo-toxicity associated with short wavelength excitation; less overlap with cellular autofluorescence (one exception being chlorophyll, which emits broadly from 650 nm). Comparison among the emission spectra suggests that red FPs such as mRFP1, mCherry, and mRFPmars can be used as optimal partners with GFP due to minimal emission overlap (Fig. 2).

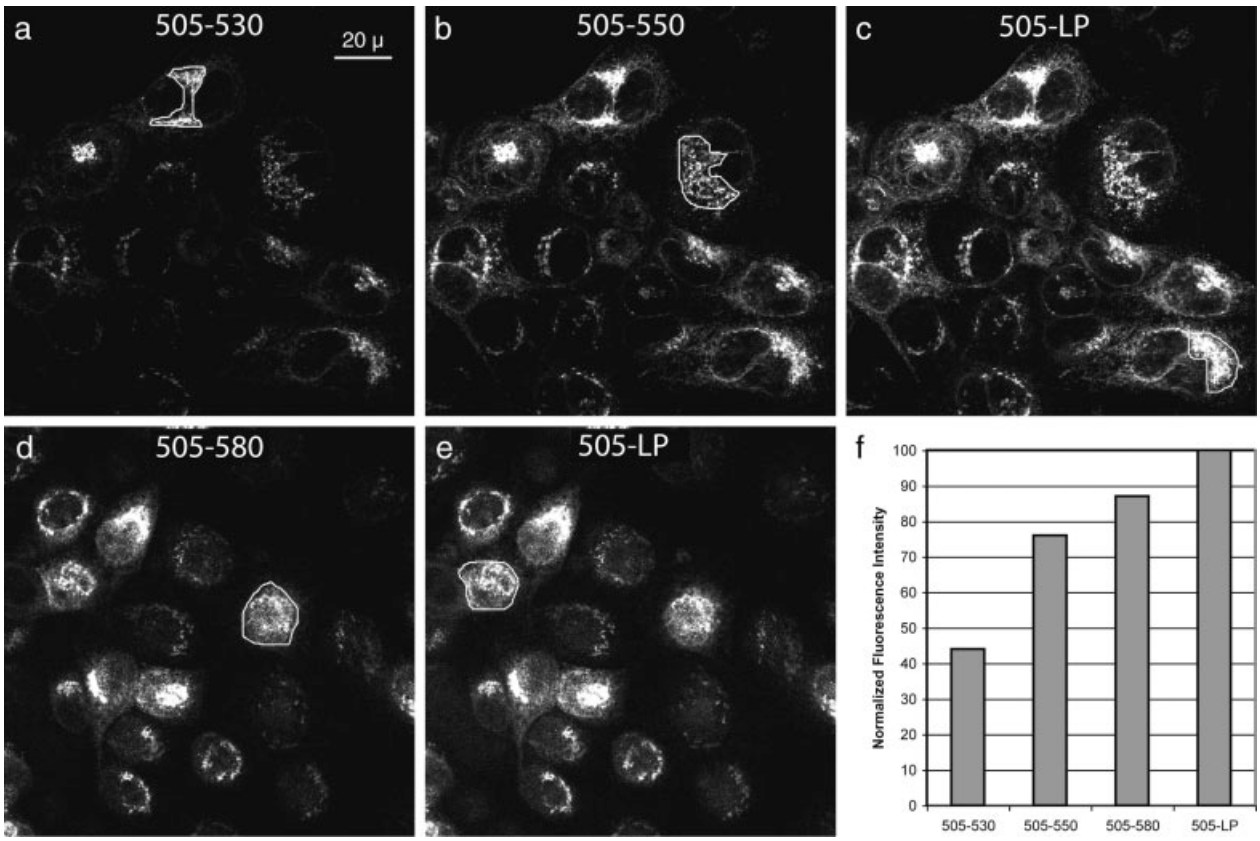

FIG. 3. GFP detection. GFP was detected using two different Zeiss LSM 510 configurations: the standard configuration for use with 488 and 543 nm excitation lines (**a**, **b**, and **c**) and the new configuration for use with 488 and 594 nm excitation lines (**d** and **e**). MDCK cells expressing VSV-G-GFP were imaged using GFP detection ranges limited so as to be useable with RFP excitation lines at (a) 543 nm (505–530 nm), (b) 561 nm (505–550 nm), or (d) 594 nm (505–580). Images in (c) and (e) were acquired using long pass 505 filters, and used to normalize values from the two different systems as percentage of LP 505. Fluorescent intensities in (**f**) represent the average of three regions within each image, indicated by white outlines.

GFP Detection

There are a limited number of laser lines available for laser scanning confocal microscopy, and an even smaller number of practical combinations for their use. Pairing of the 488 nm Argon line with a 543 nm Helium-Neon (HeNe) has long been standard for green/red excitation. Note that during simultaneous excitation of fluorophore pairs, the second laser line fundamentally limits the range over which the green fluorophore may be detected. The green detection range must be limited well below 543 nm, so that light from this laser is not detected. Because the intensity of excitation is typically many orders of magnitude higher than the resulting fluorescence, even a small percentage of laser bleed-through will quickly swamp the signal. For this reason, Zeiss specifies that the emission filter cut-on and cut-off (the wavelength at which an emission filter reaches 50% transmission) must be at least 15 nm from a laser line with which they are used. The typical green emission filter used with 488 and 543 nm excitation is therefore 505–530 (505 being 17 nm away from 488, and 530 being 13 nm away from 543), which leaves 25 nm bandwidth for detection of fluorescence emission (Fig. 3a). The combination of both 488 and 568 nm for green/red excitation in the Krypton-Argon (Kr-Ar) mixed gas laser offers some improvement, extending the range of green detection by 25 nm up to about 50 nm (Fig. 3b). However, Kr-Ar lasers suffer from a number of drawbacks, including short lifetimes and poor output stability. Once a standard configuration of the LSM 510, the Kr-Ar laser is no longer offered.

Recent progress in laser development has introduced several new lines (561 nm diode and 594 nm HeNe) to confocal use, which are promising for RFP excitation. The 561 nm diode line is available at power levels up to 25 mW, whereas the 594 nm line is available at up to a more modest 2.5 mW. Our 594 nm laser was specified by the manufacturer at 2 mW, but actual output was measured at 3.4 mW (Table 1). Excitation at 488 and 561 nm leaves a green fluorescence detection range of approximately 505–546 (Fig. 3b), roughly 40 nm. Excitation at 488 and 594 nm leaves a green detection range of approximately 505–580, roughly 75 nm (Fig. 3d). Note that the higher power of the 561 nm line means greater care must be taken to avoid excitation bleed-through into the detection channel.

RFP Excitation and Detection

The excitation peaks of the red FPs mRFP1, mRFPmars, and mCherry are 584, 585, and 587 nm respectively (Figure 4). All three have shoulders with roughly 50% of

Table 1
Output Power at the Laser Head

Laser type	Laser output (mW)	Suppliers rating (mW)
Argon (all lines)	50.2	40
He-Ne (594)	3.36	2
He-Ne (633)	6.53	5

These measurements illustrate the actual power levels that may be expected from the different laser lines when compared with the supplier's power rating. Measurement at 405 nm was not performed because the power meter detection head could not physically be inserted between the 405 nm laser head and AOTF.

the maximum absorption around 550 nm. The traditional 543 nm line does not line up well with these peaks, although excitation is still possible because of the shoulder. The 594 nm HeNe line lies between 7 and 10 nm from these excitation peaks, whereas the 561 nm line lies between 23 and 26 nm away. We chose the 594 nm line for use because excitation of RFPs at this wavelength is most efficient, and allows for the broadest range of GFP fluorescence detection. Excitation at 594 nm is also well suited for use with fluorophores such as Texas Red and Cy 3.5. Note, however, that 594 nm also excites Cy5, which is normally excited using 633 nm, causing cross talk when Cy5 is used in combination with RFP excitation at 594. Cy5.5, which is not excited at 594 nm, can be used instead of Cy5 to overcome this limit.

In keeping with the 15 nm rule (see earlier) Zeiss insisted that emission detection should be limited to above 610 nm in conjunction with 594 nm excitation. Unfortunately, this means that the emission peaks of mRFP1 and mRFPmars (607 and 602 nm respectively) are narrowly missed. The emission peak of mCherry falls at exactly 610 nm (Fig. 2). RFP detection using 594 nm excitation is therefore not as sensitive as using 561 nm excitation (Fig. 5). One option to improve red detection is to insert an LP 605 filter into the change position (position number 7 (LP 660) on EM1 or position number 6 (BP 420–500) on EM2), which catches more of the mCherry peak and improves detection to roughly 70% of maximum. Interestingly, there is little gain in mCherry sensitivity associated with detection starting at 550 nm when compared with detection starting at 575.

Assessment of Green-into-Red Crosstalk

Optimal GFP detection would be open ended starting at 505 nm, whereas optimal mCherry detection would be open ended starting around 575 nm. For simultaneous two channel imaging, the crucial question is "How much GFP signal can be detected in the different red channels associated with excitation of RFPs at 543, 561, and 594 nm?" As shown in Figure 5, GFP bleeds strongly into a 550–700 nm red detection channel, such that at similar gain settings, the red signal equals 60% of the green signal. The situation is somewhat better for RFP excitation at 561 nm, which limits the start of RFP detection to 575 nm. In this case, bleed-through of GFP into the red detection range equals 20% of the GFP signal detected in the green channel. If the red detection range is pushed to begin at 610 nm, the bleed-through of GFP is limited to 4%.

Laser Power Measurement

The HeNe laser format has been tried and tested in confocal microscopy at 543 and 633 nm; these lasers typically have long lifetimes of up to 10,000 h, relatively low maintenance, high output stability, and good beam shape for fiber optic coupling. Because the 594 HeNe laser tube shares the same physical dimensions as the 543 and 633 HeNe lasers, the 594 He-Ne can easily be placed in the

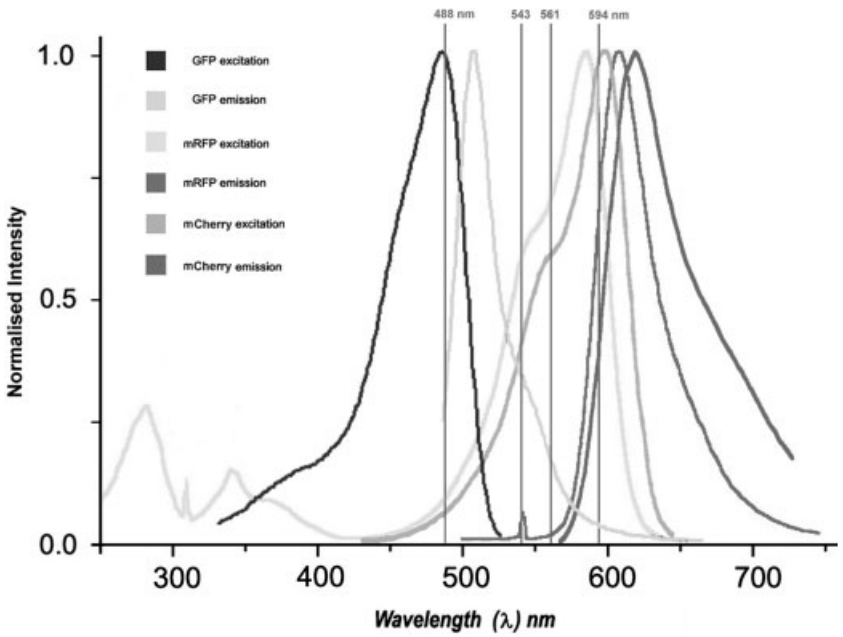

FIG. 4. Excitation and emission of GFP, mRFP1, and mCherry. Redrawn from Campbell et al. (21), Shaner et al. (23) and the Zeiss CellScience fluorophore database (http://cellscience.bio-rad.com/fluorescence/fluorophoreDatab.htm).

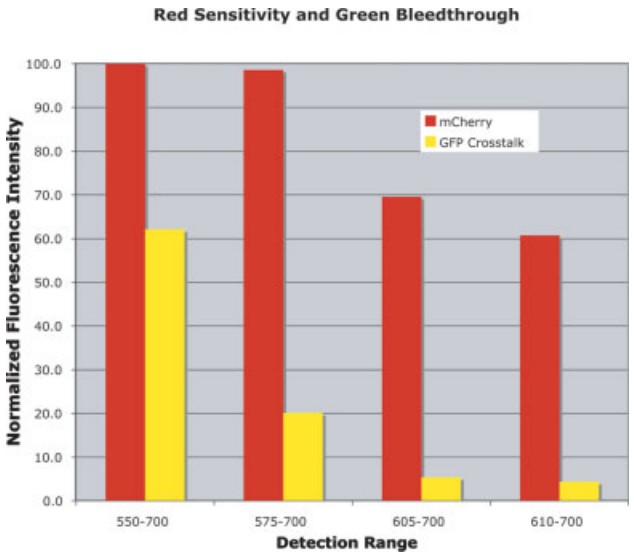

FIG. 5. mCherry detection and GFP crosstalk. mCherry-LASP was excited at 543 nm and imaged using detection ranges compatible with laser excitation at 543 nm (550–700 nm), 561 nm (575–700 nm), and 594 nm (605 and 610–700 nm). In a separate experiment, GFP-actin was excited at 488 nm and imaged using the same red detection ranges, in addition to being imaged using the standard green detection range of 505–530 nm. The PMT gain of both red and green detection channels was kept constant at 650, and the intensity of the green image was maximized by adjusting laser power. GFP crosstalk is expressed as a ratio of GFP signal detected in the red channel to GFP signal detected in the green channel.

standard laser combiners of the major commercial confocal systems. The 561 nm diode laser has a box-shaped housing that must be adapted to preexisting laser combiners. This difference may be of concern to those who wish to upgrade existing systems to include one of these two lasers. These lasers may also have issues with beam shape, which influences coupling efficiency. The 594 nm laser line exhibited constant power for more than 2 months (Table 2). This indicates that opto-mechanical integration of the HeNe laser tube was extremely stable. HeNe power measured in the specimen plane was in fact much more stable than either the 405 diode or Argon-ion laser coupling, each of which suffered at least one unexplained power loss over the course of 2 months.

DISCUSSION

Live cell imaging of two FPs is a powerful and demanding application in light microscopy. It is demanding due to the many restrains on image acquisition, including weak signals, cross talk, and photo-damage (both photo-bleaching and photo-toxicity), which must be balanced against each other to image a sample at the desired time resolution for the duration of an experiment. These parameters are inter-dependent, meaning that improvement in one generally comes at the expense of the others. Researchers engaged in the most demanding live cell experiments often find that every photon counts, that each parameter is important, and that none of them can be compromised without a loss of information. Therefore, any technique that improves one parameter without compromising the others truly increases the information that can be obtained from a living specimen.

Co-localization of proteins during dynamic events strongly suggests their joint involvement, which may be further dissected based on their times of arrival and departure during the event, turnover rates, etc. Assessment of co-localization is fundamentally limited by the ability to detect and separate fluorescence signals. This task is complicated by the generally weak signals encountered in live cell imaging and the overlapping emission spectra of many commonly used fluorophore pairs. Several techniques have been developed for the separation of overlapping emission signals from double-labeled specimens imaged by laser scanning confocal microscopy.

Table 2
Laser Power Stability at the Objective

	Measured power per line in object plane in mW						
Measurement	405[a]	458[a]	477[a]	488[a]	514[a]	594[a]	633[a]
1	2.31	0.24	0.38	1.22	0.62	0.17	0.41
2	2.44	0.2	0.32	1.05	0.5	0.17	0.38
3	2.46	0.18	0.27	0.95	0.5	0.17	0.41
4	2.27	0.12	0.18	0.59*	0.3	0.15	0.37
5	2.13	0.32	0.46	1.4	0.68	0.16	0.37
6	2.42	0.25	0.4	1.22	0.5	0.14	0.31
7	2.32	0.24	0.42	1.32	0.72	0.16	0.39
8	1.27*	0.23	0.36	1.13	0.57	0.16	0.39
Mean	2.2	0.22	0.35	1.11	0.55	0.16	0.38
SD	0.39	0.06	0.09	0.25	0.13	0.01	0.03
Stability	5.6	3.7	3.9	4.4	4.2	16.0	12.7

Measurement of seven laser lines once per week over a period of 8 weeks. Two measurements (*) indicated significant, unexplained drops in the power output of he system, which were corrected by our Zeiss service technician. In one case, the mirror directing the Argon (488 nm) laser into the fiber launch required re-alignment. In the second case, the fiber launch of the Diode (405 nm) laser required adjustment. The cause of these power drops is unknown, but might have been caused by temperature fluctuations, external vibrations, or instability of the diode laser output. Note the stability (which is expressed here as the ratio of the Mean to the Standard Deviation) is highest for the two HeNe lines at 594 and 633 nm.

[a]Values are given in nm.

Sequential Scanning

The simplest approach involves sequential channel acquisition, also called multi-tracking, which reduces the risk of cross-talk by illuminating and detecting only one fluorophore at a time. Multitracking can be used to reduce cross-talk, but the eliminated cross-talk signal still represents photons lost to the true signal. For example, multitracking of GFP and RFP depends on a secondary beam splitter in the optical path, which splits red and green signals into different detectors. A typical secondary beamsplitter associated with 561 nm excitation is NFT 565. Note that in the case of multi-tracking, this mirror will direct all GFP emission above 565 nm into the wrong detector (which will represent a larger loss of signal than the 20% crosstalk in Fig. 5). GFP signal sent to the red detector cannot be recovered. In the case of RFP excitation at 561 nm, optimal detection of GFP when multi-tracking would require inclusion of a secondary beamsplitter such as NFT 595. In this case, however, detection of the full emission of GFP would still be hindered by the use of the 488/561 primary beam splitter, due to the reflection of some GFP emission around 561 nm (Leica has recently made much of this issue with their AOBS). It is also worth noting that RFPs may be weakly excited at 488 nm (9, and unpublished observations), but this signal is thrown away during sequential scanning. Multi-tracking also increases the time required to acquire an image because each image point must be scanned twice. Time resolution is therefore roughly half of the case for simultaneous acquisition of both channels. Finally, the software set-up for sequential scanning is slightly more complex than for simultaneous two channel acquisition, which may hinder its correct use among novice microscopists and add to the work load of the staff running a multi-user facility.

Linear Unmixing

Linear unmixing techniques for imaging fluorophores with overlapping emission spectra are now well established (24). These approaches are based on the use of reference emission spectra from individual fluorophores to mathematically deconvolve the mixed emission spectrum of the pair. On a technical level, the utility of linear unmixing for weak FPs is limited by factors such as the image background level, noise, and the relationship of the emission peaks to the detection channels (25). Our experience with linear unmixing hardware and software from Leica, Zeiss, and Olympus has led us to view linear unmixing with caution. These are a group of specialized techniques, requiring detailed knowledge of the fluorophores and samples involved, of the spectral characteristics of imaging system, and of the theoretical principles behind spectral deconvolution, which may be ill suited for novices. As with image deconvolution, it is much easier to get an answer than to be sure you have the correct answer. We have found considerable practical difficulty even in the separation of GFP from YFP using the Zeiss META-detector, an example which highlights many shortcomings of the spectral unmixing approach. The first generation META detector showed lower sensitivity because of increased noise when compared with standard PMTs, which limits imaging applications with low fluorescent signals. Second, the spectral unmixing algorithm requires that both fluorophore signals must be within the dynamic range of the detector at one gain setting. The spectral detector, with 32 miniature PMTs in series, behaves as a single unit having one gain control. If the emission of one fluorophore is significantly brighter than the other (which is frequently the case where GFP and YFP are coexpressed in living cells), then it is very difficult to keep both signals within the dynamic range of a constant gain setting for the detector. The algorithm for spectral unmixing cannot then be applied with complete success. Finally, the signal-to-noise ratio of an image may be degraded by detection of a fluorophore's complete emission spectrum as multiple spectral bands, each having a fraction of the intensity of the complete emission spectrum. Spectral unmixing works best when two signals are strong and more-or-less equal, which is the exception rather than the rule for FP imaging. It is worth noting that a second generation Meta detector has recently been released, which should offer some improvements in sensitivity and variability of gain.

Simultaneous Optical Separation

Recent advances in FP and laser technology mean that FP pairs now exist, which can be unambiguously separated based on their excitation and emission properties. There are several advantages to the traditional approach to spectral separation based on selective excitation and emission detection, when compared with linear unmixing or multi-tracking approaches. The most obvious advantage is minimized risk of artifact due to the simplicity of the traditional approach. Furthermore, no special training beyond fluorescence microscopy basics is required. (For the staff running a multi-user environment, this advantage is multiplied by the number of users.) Finally, the traditional approach offers superior speed and sensitivity over other approaches to spectral detection and multi-tracking. Building up a spectrum with a scanning emission detector takes time. In our view, direct optical separation of two colors based on selective detection offers greater flexibility and sensitivity when compared with either sequential acquisition or linear unmixing.

LSM 510 Hardware Version 3.2 Versus Version 3.5

No microscope configuration can perfectly address all the requirements of every application. Removal of the 543 nm laser prohibits the excitation of common red fluorophores such as Cy3 and TRITC. The 543 nm line was sacrificed because hardware version 3.2 of the Zeiss laser module could only incorporate up to three lasers through the VIS port (in addition to the 405 nm blue diode coupled via the UV port). The new version of the LSM 510 hardware, version 3.5, allows incorporation of more than three visible lasers. In principle this means that a wider selection of lasers can be used together; however, the selection

and placement of mirrors, especially the primary and secondary beamsplitters, remains a practical consideration.

The 561 nm Laser Line

The 561 nm diode laser line was not available during the specification of this system. This line is now an alternative to the 594 nm line for excitation of some red-shifted fluorophores. Excitation at 561 nm is somewhat less efficient for longer wavelength RFPs; however, this excitation inefficiency is offset by the extra power (10 mW) of the 561 nm line. Although excitation of RFPs at 561 nm restricts the range of emission detection for GFP, an HFT primary dichroic mirror for 405/488/561/633 excitation more evenly divides the emission spectrum between 488 and 633 nm and is clearly advantageous for four-color imaging. The 561 nm line is undoubtedly a useful addition to the list of lasers available for confocal use. However, the extreme opto-mechanical stability of the HeNe laser is not to be overlooked (Table 2), especially for the staff running a multi-user facility.

SUMMARY

We have specified a configuration of the Zeiss LSM 510 for simultaneous imaging of two FPs: GFP and red variants such as mCherry. This configuration has been optimized for maximum sensitivity and minimum cross talk during live cell imaging, based on the use of fluorophores with nonoverlapping emission spectra (Fig. 6). To maximize the range over which GFP can be detected, we selected a 594 nm HeNe as the red fluorophore excitation source. Measured in the specimen plane, 594 nm laser has roughly two times the power of standard 543 nm laser: 0.16 mW versus 0.07 mW. 594 nm is useful for the excitation of red-shifted RFPs and other fluorophores such as Texas Red and Cy 3.5. The wide spacing between the 488 and 594 nm excitation lines ensures detection of nearly the entire GFP emission curve and minimum signal loss (13%) when compared with long pass detection. Detection of the widest possible GFP emission range also minimizes the risk of green-into-red cross talk. Because mCherry is excited at 594 nm, emission can be first detected at 610 nm, by which point GFP emission is virtually undetectable. Imaging, however, involves compromises. In this configuration, detection of GFP (the brighter fluorophore) and green-into-red crosstalk have been optimized at the expense of detection of mCherry (the dimmer fluorophore), which is 60–70% of the signal which would be detected using a range compatible with excitation at 561 nm (Fig. 6. Note, however, that GFP detection is 10% dimmer when 561 nm excitation is employed, due to the restricted detection range). We feel this compromise is justified by the reduced risk of crosstalk, which can lead to the dangerous false positive indication of co-localization between red and green-labeled proteins. Because the green is the brightest of the two FPs, a small amount of green bleed through is more likely to be detected as false positive in the red channel. Careful experimental design, i.e. labeling the weaker protein with the brighter fluorophore, is also important to maximize sensitivity and minimize crosstalk. For example, actin meshworks are dense structures, which can be easily imaged with RFPs. Proteins, which regulate actin polymerization, are present at the leading edge of a growing meshwork in much smaller amounts, and are therefore optimally labeled with GFP, the brighter fluorophore (unpublished observations). Our hope and expectation is that red fluorophores having slightly red-shifted emission peaks will emerge. Red-shifting the emission of mCherry by even 10 nm would shift the half-maximum peak value to 605 nm, which would substantially improve detection of the entire mCherry emission curve and further minimize the risk of GFP crosstalk. An increase in quantum yield would also be a desirable improvement. Such a brighter, red-shifted mCherry would undoubtedly become the standard fluorophore partner to GFP because of the ability to capture all photons from both probes simultaneously with no risk of false co-localization. Alternatively, risk of crosstalk would also be minimized if the emission range of GFP could be narrowed. Then existing RFPs such as mCherry could be excited at 561 without limiting the GFP detection range, and RFPs could be detected starting at 575 nm without the risk of 20% green-into-red crosstalk. It is not clear, however, if the emission range of GFP could be modified without sacrificing overall fluorescence yield (i.e. brightness).

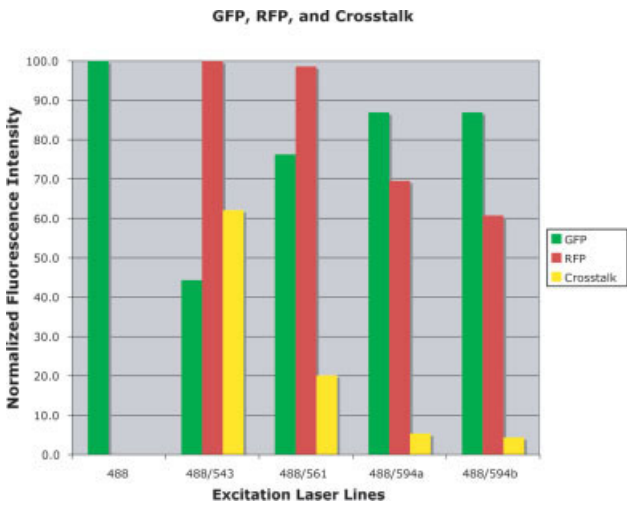

FIG. 6. Comparison of GFP, mCherry, and crosstalk. The relative signal strengths of GFP, mCherry, and green-into-red crosstalk are compared using the following detection channels: 488, long pass 505 detection of green only; 488/543, detection of green at 505–530 nm, detection of red at 550–700 nm; 488/561, detection of green at 505–550 nm, detection of red at 575–700 nm; 488/594a, detection of green at 505–580, detection of red at 605–700 nm; 488/594b, detection of green at 505–580, detection of red at 610–700 nm. Green detection is maximized when using 488/594 excitation, whereas red detection is maximized using 488/561 excitation. However, green-into-red crosstalk represents 20% of maximum red signal intensity when 488/561 nm excitation is used, whereas crosstalk is reduced to 4 and 5% when 488/594 nm excitation is used with red detection starting at 610 and 605 nm respectively.

The wide spacing of the 488 and 594 nm lines is a strength of the system with regard to green and red FP imaging, but necessarily limits the utility for green-red FRET, which depends on overlapping emission and excita-

tion spectra of the shorter and longer wavelength fluorophores respectively. However, CFP, YFP, and CFP-YFP FRET can still be imaged normally. We hope this configuration will be of use to researchers, especially in multi-user environments, needing a robust system for simple, sensitive, two-color FP imaging.

ACKNOWLEDGMENTS

The system configuration was prepared in collaboration with Carmen Brückner, Dr. Volker Jüngel, and Frank-Peter Schoew (Carl Zeiss AG, Jena). The protocol for the laser power measurement was prepared with the help of Hendrik Merkel (Carl Zeiss AG, Jena). We are grateful to Mario Kreissl for excellent support, and the many users of the MPI-CBG-LMF who challenged us to get the most out of this system, especially Jochen Rink, Laki Pantazis, and Christian Bökel.

LITERATURE CITED

1. Wang Y-L. Fluorescent analog cytochemistry. In: Wang Y-L, Taylor DL, editors. Fluorescence Microscopy of Living Cells in Culture, Part A: Fluorescent Analogs, Labeling Cells, and Basic Microscopy, New York: Academic Press; 1989. Methods in Cell Biology, Vol. 29, pp 1–12.
2. Taylor DL, Wang YL. Fluorescently labelled molecules as probes of the structure and function of living cells. Nature 1980;284:405–410.
3. Prasher DC, Eckenrode VK, Ward WW, Prendergast FG, Cormier MJ. Primary structure of the Aequorea victoria green-fluorescent protein. Gene 1992;111:229–233.
4. Chalfie M, Tu Y, Euskirchen G, Ward WW, Prasher DC. Green fluorescent protein as a marker for gene expression. Science 1994;263:802–805.
5. Miyawaki A, Sawano A, Kogure T. Lighting up cells: Labelling proteins with fluorophores. Nat Cell Biol 2003; (Suppl):S1–S7.
6. Lippincott-Schwartz J, Patterson GH. Development and use of fluorescent protein markers in living cells. Science 2003;300:87–91.
7. Tsien RY. The green fluorescent protein. Annu Rev Biochem 1998;67:509–514.
8. Wang Y-L. Exchange of actin subunits at the leading edge of living fibroblasts: Possible role of treadmilling. J Cell Biol 1985;101:597–602.
9. Krylyshkina O, Anderson KI, Kaverina I, Upmann I, Manstein DJ, Small JV, Toomre DK. Nanometer targeting of microtubules to focal adhesions. J Cell Biol 2003;161:853–859.
10. Benesch S, Polo S, Lai FP, Anderson KI, Stradal TE, Wehland J, Rottner K. N-WASP deficiency impairs EGF internalization and actin assembly at clathrin-coated pits. J Cell Sci 2005;118(Part 14):3103–3115.
11. Gerisch G, Bretschneider T, Muller-Taubenberger A, Simmeth E, Ecke M, Diez S, Anderson K. Mobile actin clusters and travelling waves in cells recovering from actin depolymerization. Biophys J 2004;87: 3493–3503.
12. Day RN. Imaging protein behavior inside the living cell. Mol Cell Endocrinol 2005;230:1–6.
13. Michalet X, Pinaud FF, Bentolila LA, Tsay JM, Doose S, Li JJ, Sundaresan G, Wu AM, Gambhir SS, Weiss S. Quantum dots for live cells, in vivo imaging, and diagnostics. Science 2005;307:538–544.
14. Remington SJ. Negotiating the speed bumps to fluorescence. Nat Biotechnol 2002;20:28,29.
15. Shaner NC, Steinbach PA, Tsien RY. A guide to choosing fluorescent proteins. Nat Methods 2005;2:905–909.
16. Patterson G, Day RN, Piston D. Fluorescent protein spectra. J Cell Sci 2001;114(Part 5):837,838.
17. Verkhusha VV, Lukyanov KA. The molecular properties and applications of Anthozoa fluorescent proteins and chromoproteins. Nat Biotechnol 2004;22:289–296.
18. Vieira OV, Verkade P, Manninen A, Simons K. FAPP2 is involved in the transport of apical cargo in polarized MDCK cells. J Cell Biol 2005; 170:521–526.
19. Zucker RM, Price O. Evaluation of confocal microscopy system performance. Cytometry 2001;44:273–294.
20. Fradkov AF, Chen Y, Ding L, Barsova EV, Matz MV, Lukyanov SA. Novel fluorescent protein from Discosoma coral and its mutants possesses a unique far-red fluorescence. FEBS Lett 2000;479:127–130.
21. Campbell RE, Tour O, Palmer AE, Steinbach PA, Baird GS, Zacharias DA, Tsien RY. A monomeric red fluorescent protein. Proc Natl Acad Sci USA 2002;99:7877–7882.
22. Fischer M, Haase I, Simmeth E, Gerisch G, Muller-Taubenberger A. A brilliant monomeric red fluorescent protein to visualize cytoskeleton dynamics in Dictyostelium. FEBS Lett 2004;577:227–232.
23. Shaner NC, Campbell RE, Steinbach PA, Giepmans BN, Palmer AE, Tsien RY. Improved monomeric red, orange and yellow fluorescent proteins derived from Discosoma sp. red fluorescent protein. Nat Biotechnol 2004;22:1567–1572.
24. Zimmermann T. Spectral imaging and linear unmixing in light microscopy. Adv Biochem Eng Biotechnol 2005;95:245–265.
25. Zimmermann T, Rietdorf J, Pepperkok R. Spectral imaging and its applications in live cell microscopy. FEBS Lett 2003;546:87–92.